

# Time Varying Channel Tracking for Multi-UAV Wideband Communications with Beam Squint

Jianwei Zhao, Qi Dong, Yanjie Zhao, Bolei Wang, and Feifei Gao

**Abstract**—Unmanned aerial vehicle (UAV) has become an appealing solution for a wide range of commercial and civilian applications because of its high mobility and flexible deployment. Due to the continuous UAV navigation, the channel between UAV and base station (BS) is subject to the Doppler effect. Meanwhile, when the BS is equipped with massive number of antennas, the non-negligible propagation delay across the array aperture would cause beam squint effect. In this paper, we first investigate the channel of UAV communications under both Doppler shift effect and beam squint effect. Then, we design a gridless compressed sensing (GCS) based channel tracking method, where the high dimension uplink channel can be derived by estimating a few physical parameters such as the direction of arrival (DOA), Doppler shift, and the complex gain information. Besides, with the Doppler shift reciprocity and angular reciprocity, the downlink channel can be derived by only one pilot symbol, which greatly decreases the downlink channel training overhead. Various simulation results are provided to verify the effectiveness of the proposed methods.

**Index Terms**—UAV, massive MIMO, beam squint, time varying channel, and channel tracking.

## I. INTRODUCTION

Unmanned aerial vehicle (UAV) has attracted ever increasing attention from both the industry and the academia due to its high mobility and flexible deployment. UAVs have been widely exploited in many applications such as the transportation of good, border surveillance, search and rescue missions as well as disaster response, etc [1], [2]. Various UAV applications put forward exceptionally stringent communication requirements along the lines of available data rate, connection reliability, and latency, which promotes UAV communications with massive array antennas under millimeter-wave (mmWave) band (30GHz-300GHz) to enhance the system performance. Different from the traditional low frequency bands (< 6GHz), the mmWave has large available frequency resources that could be directly transmitted into the system bandwidth and realize broadband communications. Meanwhile, large antenna array is capable of providing enormous spatial gain, which can be utilized to overcome the large path loss of mmWave band [3]–[5].

Different from the conventional cellular communications, the majority of the UAV channel power would be contained within the line of sight (LoS) path, which motivates a lot of

angle domain signal processing studies. The authors in [6] formulated the dynamic massive MIMO channel as one sparse signal model and developed an expectation maximization (EM) based sparse Bayesian learning (SBL) framework to learn the model parameters of the sparse channel. An angle division multiple access (ADMA) based channel tracking method was proposed in [7] for massive MIMO systems, where tracking the channel is simplified to tracking the direction of arrival (DOAs) of the incident signals. Meanwhile, the uplink cooperative NOMA was investigated in [8] for cellular-connected UAV, which exploits the existing backhaul links among base stations to improve the throughput gains. The authors in [9] proposed interference alignment and soft-space-reuse based cooperative transmission for multi-cell massive MIMO networks. The authors in [10] proposed an energy-efficient UAV communication strategy via optimizing the UAV's trajectory.

However, the channel of UAV communications with massive array antenna exhibits several unique features compared to the conventional MIMO system, which hardens the procedure of channel tracking: (i) a practical channel of UAV communications would encounter Doppler shift due to the continuous UAV navigation; (ii) as with massive MIMO configuration, there would be a non-negligible propagation delay across the array aperture for the same data symbol, causing beam squint effect in frequency domain. Recently, there do exist some works [11] considering the static massive MIMO with beam squint. However, channel tracking under both Doppler shift effect and beam squint effect has not been investigated, for UAV communication systems to the best of the authors' knowledge.

In this paper, we first model the UAV communications under both Doppler shift effect and beam squint effect. Then, we present an efficient gridless compressed sensing (GCS) based channel tracking method, where tracking the spatial channel is converted to tracking the DOA of the incident signal, Doppler shift, and complex gain respectively. Additionally, the downlink channel can be derived by only one pilot symbol with the Doppler shift and angular reciprocity. Various simulation results are provided to verify the effectiveness of the proposed studies.

## II. SYSTEM AND CHANNEL MODEL

We consider multiple UAV communications with mmWave massive MIMO, where the ground base station (BS) is equipped with the  $M^B \times 1$  uniform linear array (ULA), and  $K$  UAVs are separately equipped with  $M^U \times 1$  ULA, as shown

J. Zhao, B. Wang, and F. Gao are with Tsinghua National Laboratory for Information Science and Technology (TNList) Beijing 100084, P. R. China (e-mail: zhaojw15@mails.tsinghua.edu.cn, boleiwang@ieee.org, feifeigao@ieee.org). J. Zhao is also with High-Tech Institute of Xi'an, Xi'an, Shaanxi 710025, China. Q. Dong, and Y. Zhao are with China Academy of Electronics and Information Technology, Beijing 100041, China (e-mail: dongqiouc@126.com, zhaoyj\_dky@163.com).

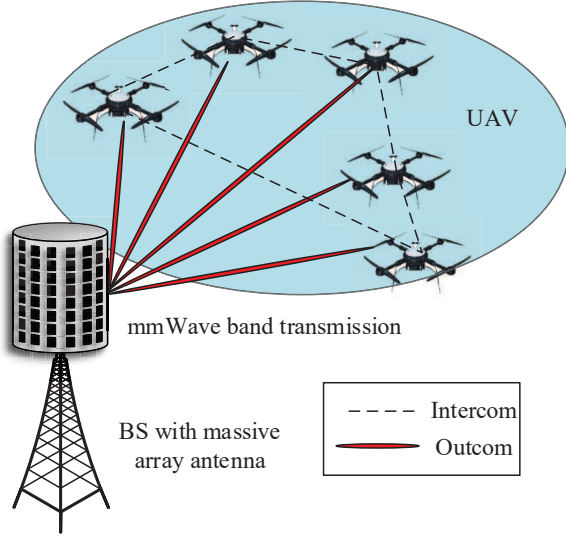


Fig. 1. System Model.

in Fig. 1. Due to the scarce scatters in the sky, the channel is naturally sparse and there are only a few incident paths on both UAV and BS side. The large path loss of mmWave band further strengthens the channel sparsity, such that the line of sight (LOS) path is dominant, while the other non-line of sight (NLOS) paths can be ignored [12], [13]. Meanwhile, due to the continuing UAV movements, the emitted wave goes through the Doppler effect.

As is shown in Fig. 2, when the  $(n+1)$ -th antenna of UAV  $k$  transmits the signal  $s_k(t)$ , the baseband signal received by the  $(m+1)$ -th antenna of BS from the  $(n+1)$ -th antenna of UAV  $k$  can be denoted as [14], [15]

$$y_{knm}(t) = s_k \left( t - m \frac{d \sin \theta_k^B}{c} - n \frac{d \sin \theta_k^U}{c} \right) \alpha_k e^{-j2\pi f_{kd}t} e^{-j2\pi m \frac{d \sin \theta_k^B f_c}{c}} e^{-j2\pi n \frac{d \sin \theta_k^U f_c}{c}}, \quad (1)$$

where  $\alpha_k$  is the channel gain,  $f_{kd}$  is the Doppler shift,  $d$  is the distance between two adjacent antennas,  $c$  is the light speed,  $\theta_k^B$  and  $\theta_k^U$  are the DOA at BS and the direction of departure (DOD) of UAV respectively, and  $f_c$  is the carrier frequency.

For the traditional narrow band MIMO systems, the antenna numbers  $M^B$  and  $M^U$  are finite, and meanwhile the symbol duration  $T_s$  is relatively large. Hence, the following inequality always holds that

$$m \frac{d \sin \theta_k^B}{c} + n \frac{d \sin \theta_k^U}{c} \ll T_s \quad (2)$$

and Equ. (1) reduces to

$$y_{knm}(t) \approx s(t) \alpha_k e^{-j2\pi f_{kd}t} e^{-j2\pi m \frac{d \sin \theta_k^B f_c}{c}} e^{-j2\pi n \frac{d \sin \theta_k^U f_c}{c}}. \quad (3)$$

In this case, the effective uplink channel between the  $(n+1)$ -th antenna of UAV  $k$  and the  $(m+1)$ -th antenna of the ground

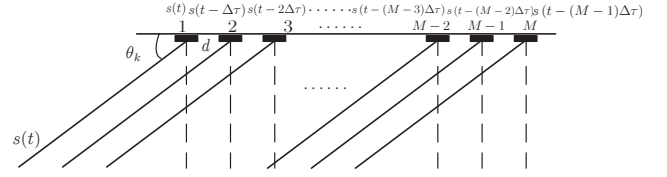


Fig. 2. System Model.

BS can be expressed

$$h_{k,n,m} = \alpha_k e^{-j2\pi f_{kd}t} e^{-j2\pi m \frac{d \sin \theta_k^B f_c}{c}} e^{-j2\pi n \frac{d \sin \theta_k^U f_c}{c}}, \quad (4)$$

and the corresponding channel matrix can be derived as

$$\mathbf{H}_k = \alpha_k e^{-j2\pi f_{kd}t} \mathbf{a}(\theta_k^B) \mathbf{a}^T(\theta_k^U), \quad (5)$$

where  $\mathbf{a}(\theta_k^B)$  is the  $M^B \times 1$  steering vector at BS side with  $[\mathbf{a}(\theta_k^B)]_m = e^{-j \frac{2\pi m d \sin \theta_k^B}{\lambda_c}}$ , while  $\mathbf{a}(\theta_k^U)$  is the  $M^U \times 1$  steering vector at UAV side with  $[\mathbf{a}(\theta_k^U)]_n = e^{-j \frac{2\pi n d \sin \theta_k^U}{\lambda_c}}$ .

However, under massive MIMO configuration and large bandwidth of mmWave, the time delay of the signals across the large antenna array cannot be ignored. Hence, there could be

$$m \frac{d \sin \theta_k^B}{c} + n \frac{d \sin \theta_k^U}{c} > T_s, \quad (6)$$

and the approximation in Equ. (3) does not hold. In this case, different antenna would see unsynchronized  $s_k(t)$  and the conventional MIMO model (5) is not valid anymore. The corresponding phenomenon can be named as *beam squint* effect [11].

Under both the Doppler shift effect and beam squint effect, the uplink channel between the  $(m+1)$ -th antenna of the ground BS and the  $(n+1)$ -th antenna of UAV should be modeled as [14], [15]

$$h_{k,n,m} = \alpha_k e^{-j2\pi f_{kd}t} e^{-j2\pi m \frac{d \sin \theta_k^B f_c}{c}} e^{-j2\pi n \frac{d \sin \theta_k^U f_c}{c}} \delta \left( \tau - m \frac{d \sin \theta_k^B}{c} - n \frac{d \sin \theta_k^U}{c} \right), \quad (7)$$

while the corresponding frequency response can be derived as

$$h_{k,n,m}(f) = \int_{-\infty}^{+\infty} h_{k,l,m} e^{-j2\pi f \tau} d\tau = \alpha_k e^{-j2\pi f_{kd}t} e^{-j2\pi m \frac{d \sin \theta_k^B f_c}{c}} e^{-j2\pi n \frac{d \sin \theta_k^U f_c}{c}} e^{-j2\pi f m \frac{d \sin \theta_k^B}{c}} e^{-j2\pi f n \frac{d \sin \theta_k^U}{c}}. \quad (8)$$

It can be readily derived that the continuous time-frequency MIMO channel is

$$\mathbf{H}_k(t, f) = \alpha_k e^{-j2\pi f_{kd}t} \mathbf{a}(\theta_k^B, f) \mathbf{a}^T(\theta_k^U, f), \quad (9)$$

where  $\mathbf{a}(\theta_k^B, f)$  is the  $M^B \times 1$  spatial steering vector at BS side with

$$[\mathbf{a}(\theta_k^B, f)]_m = e^{-j \frac{2\pi m d \sin \theta_k^B}{\lambda_c} (1 + \frac{f}{f_c})}, \quad (10)$$

while  $\mathbf{a}(\theta_k^U, f)$  is the  $M^U \times 1$  spatial steering vector at UAV side with

$$\left[\mathbf{a}(\theta_k^U, f)\right]_n = e^{-j\frac{2\pi n d \sin \theta_k^U}{\lambda_c}(1 + \frac{f}{f_c})}. \quad (11)$$

*Remark 1:* To the best of the authors knowledge, this is the first work that presents the channel modeling of massive MIMO system under both the Doppler shift effect and beam squint effect for UAV communications.

For ease of illustration, we assume that each UAV is equipped with  $M^U = 1$  antenna in the rest of this paper. Then the continuous-time channel could be simplified as

$$\mathbf{H}_k(t, f) = \alpha_k e^{-j2\pi f d t} \mathbf{a}(\theta_k, f), \quad (12)$$

where  $\theta$  is DOA of the incident signals at BS side.

The discrete-time channel at block  $l$  could be derived as

$$\mathbf{h}_k(l, f) = \alpha e^{-j2\pi f_{kd} l N_b T_s} \mathbf{a}(\theta_k, f), \quad (13)$$

where  $N_b$  is the number of symbols in each block.

Since the UAV speed and physical location would change much slower than the channel variation, the UAV movement related parameters such as  $f_{kd}$  and  $\theta_k$  can be viewed as unchanged within tens of blocks. Therefore, we can stack channels of  $L$  blocks into an  $LM \times 1$  vector  $\mathbf{h}_k(f)$  and obtain

$$\begin{aligned} \mathbf{h}_k(f) &= \alpha_k \text{vec} \left[ \mathbf{a}(\theta_k, f) \mathbf{b}^H(f_{kd}) \right] \\ &= \alpha_k \mathbf{p}(f_{kd}, \theta_k, f), \end{aligned} \quad (14)$$

where  $\mathbf{b}(f_{kd}) = [1, e^{-j2\pi f_{kd} N_b T_s}, \dots, e^{-j2\pi f_{kd} (L-1) N_b T_s}]$  can be deemed as the Doppler steering vector.

Interestingly, even for LoS scenario, the large array would still lead to the inter symbol interference (ISI) due to the propagation delays of the symbols across the large antenna array, which is a significantly different phenomenon from the conventional case.

Let us apply orthogonal frequency division multiplexing (OFDM) to remove ISI. Denote  $\eta = \frac{W}{N}$  as the carrier interval, where  $W$  is the system bandwidth and  $N$  is the number of the carriers. According to Equ. (14), the channel at the  $(p+1)$ -th carrier can be expressed as

$$\mathbf{h}_k((p+1)\eta) = \alpha \mathbf{p}(f_{kd}, \theta_k, p\eta). \quad (15)$$

Since the channel model is significant for the subsequent channel tracking, precoding, and transmission, we here provide an explicit classification rule to determine the channel model type for UAV communications: nonselective, time selective, antenna selective or doubly selective.<sup>1</sup> According to (9), the antenna selective effect would not exist, when the total time delay of the signal across the massive array meets  $\frac{(M-1)d \sin \theta_k}{c} \ll T_s$ , namely,  $\frac{(M-1)d \sin \theta_k}{c T_s} \ll 1$ . Therefore, the classification rule can be readily derived as

$$\max \frac{(M-1)d \sin \theta_k}{c T_s} = \frac{(M-1)d}{c T_s} \ll 1. \quad (16)$$

Meanwhile, there would exist time selective effect when  $f_{d \max} T_s \ll 1$ , and otherwise not. Therefore, the integrated channel classification rule can be seen in Tab. I.

<sup>1</sup>Doubly selectivity here means antenna selectivity plus time selectivity.

TABLE I  
CHANNEL CLASSIFICATION RULES.

Classification Rule	$\frac{Md}{cT_s}$	$f_{d \max} T_s$
nonselective	$\ll 1$	$\ll 1$
antenna selective	$\geq 1$	$\ll 1$
time selective	$\ll 1$	$\geq 1$
doubly selective	$\geq 1$	$\geq 1$

*Theorem 1:* Under the condition  $M^B \rightarrow \infty$  and  $L \rightarrow \infty$ , the channels  $\mathbf{h}_k((p+1)\eta)$  in Equ. (14) are progressively orthogonal for UAV communications with mmWave massive array antenna when UAVs have distinct DOAs or velocities.

*Proof 1:* When  $M^B \rightarrow \infty$  and  $L \rightarrow \infty$ , the relationship between  $\mathbf{h}_1^H((p+1)\eta)$  and  $\mathbf{h}_2((p+1)\eta)$  meets (17), which is shown on the top of the next page. Moreover,  $\xi_k$  is given by

$$\xi_k = \left[ \frac{d(\sin \theta_1 - \sin \theta_2)}{\lambda_c} + p\eta \frac{d(\sin \theta_1 - \sin \theta_2)}{c} \right]. \quad (17)$$

Therefore, the channels  $\mathbf{h}_k((p+1)\eta)$  in Equ. (14) are progressively orthogonal for UAV communications when the UAVs have distinct DOAs or velocities.

According to Theorem 1, the sparse characteristic of UAV communications with mmWave massive array antenna makes it possible to schedule users according to the channel DOA or velocity information. As is vividly shown in Fig. 3, the users with different DOA or velocity could be simultaneously scheduled. The corresponding user scheduling scheme can be named as angle division multiple access (ADMA) and velocity division multiple access (VDMA).

### III. CHANNEL TRACKING STRATEGY

The beam squint effect makes the traditional channel transmission strategy inapplicable for UAV communications with mmWave massive array antenna. In this section, we will provide a GCS based channel tracking method for UAV communications with mmWave massive array antenna.

#### A. Uplink Channel Tracking

We here utilize the comb-type pilot channel estimation to track the time-varying channel. Let us assume  $P$  of  $N_c$  subcarriers are exploited as pilots, and the corresponding subcarrier index set for user  $k$  is  $\mathcal{P}_k = \{p_{k,1}, \dots, p_{k,P}\}$ . Then, the channel of user  $k$  in these pilot subcarrier can be stacked into a matrix as

$$\begin{aligned} \mathbf{H}_k &= \alpha_k [\mathbf{p}(f_{kd}, \theta_k, 0), \dots, \mathbf{p}(f_{kd}, \theta_k, (P-1)\eta)] \\ &= \mathbf{P}(\theta_k, f_{kd}) \alpha_k. \end{aligned} \quad (19)$$

Assuming that all users send pilot symbol “1” over the selected sub-carriers while transmitting data symbols over other sub-carriers. Then, the received uplink pilots from the  $M$  antennas and  $P$  subcarriers over  $L$  blocks can be derived as

$$\mathbf{Y} = \sum_{k=1}^K \mathbf{H}_k \mathbf{X} + \mathbf{W}, \quad (20)$$



reaches  $\lambda_{\min}$ , and  $\lambda_0$  remains fixed to balance between the sparsity and the data-fitting deviation.

By exploiting the maximization-minimization (MM) iterative method [16], the surrogate function  $S_0(\boldsymbol{\alpha}|\boldsymbol{\alpha}^{(n)})$  can be derived to minimize in the iterations of maximizing  $J_0(\boldsymbol{\alpha})$ , which is given by

$$\sum_{k=1}^K \left[ \left( \left| [\boldsymbol{\alpha}^{(n)}]_k \right|^2 + \epsilon \right) + \frac{\left( \left| [\boldsymbol{\alpha}]_k \right|^2 + \epsilon \right) - \left( \left| [\boldsymbol{\alpha}^{(n)}]_k \right|^2 + \epsilon \right)}{\left| [\boldsymbol{\alpha}^{(n)}]_k \right|^2 + \epsilon} \right] \geq J_0(\boldsymbol{\alpha}), \quad (27)$$

where  $\boldsymbol{\alpha}^{(n)}$  is the estimated value of the complex gain at the  $n$ -th iteration.

The last inequality in (27) results from the convexity of  $-J_0(\boldsymbol{\alpha})$ , and the equality will be attained only when  $\boldsymbol{\alpha}^{(n)} = \boldsymbol{\alpha}$ . Therefore, at the  $(n+1)$ -th iteration, it will hold that

$$S_0(\boldsymbol{\alpha}|\boldsymbol{\alpha}^{(n)}) - J_0(\boldsymbol{\alpha}) \geq S_0(\boldsymbol{\alpha}^{(n)}|\boldsymbol{\alpha}^{(n)}) - J_0(\boldsymbol{\alpha}^{(n)}). \quad (28)$$

Then, the optimization problem can be transformed into

$$\begin{aligned} \min_{\boldsymbol{\theta}, \boldsymbol{f}_d, \boldsymbol{\alpha}} S_\lambda(\boldsymbol{\theta}, \boldsymbol{f}_d, \boldsymbol{\alpha}|\boldsymbol{\alpha}^{(n)}) \\ = S_0(\boldsymbol{\alpha}|\boldsymbol{\alpha}^{(n)}) + \lambda \|\mathbf{y} - \boldsymbol{\alpha}\mathbf{P}(\boldsymbol{\theta}, \boldsymbol{f}_d)\|_2^2 \\ = \sum_{k=1}^K \frac{\left| [\boldsymbol{\alpha}]_k \right|^2}{\left| [\boldsymbol{\alpha}^{(n)}]_k \right|^2 + \epsilon} + \lambda \|\mathbf{y} - \boldsymbol{\alpha}\mathbf{P}(\boldsymbol{\theta}, \boldsymbol{f}_d)\|_2^2 + C(\boldsymbol{\alpha}^{(n)}), \end{aligned} \quad (29)$$

where  $C(\boldsymbol{\alpha}^{(n)})$  is a constant that is independent of  $\boldsymbol{\theta}, \boldsymbol{f}_d, \boldsymbol{\alpha}$ .

We denote  $\mathbf{D}^{(n)} = \text{diag} \left\{ \frac{\left| [\boldsymbol{\alpha}]_1 \right|^2}{\left| [\boldsymbol{\alpha}^{(n)}]_1 \right|^2 + \epsilon}, \dots, \frac{\left| [\boldsymbol{\alpha}]_{K_i} \right|^2}{\left| [\boldsymbol{\alpha}^{(n)}]_{K_i} \right|^2 + \epsilon} \right\}$ , and it can be readily derived that

$$S_\lambda(\boldsymbol{\theta}, \boldsymbol{f}_d, \boldsymbol{\alpha}|\boldsymbol{\alpha}^{(n)}) = \boldsymbol{\alpha}^H \mathbf{D}^{(n)} \boldsymbol{\alpha} + \lambda \|\mathbf{y} - \boldsymbol{\alpha}\mathbf{P}(\boldsymbol{\theta}, \boldsymbol{f}_d)\|_2^2 + C(\boldsymbol{\alpha}^{(n)}). \quad (30)$$

According to the above analysis, we can further compute that

$$\begin{aligned} J_\lambda(\boldsymbol{\theta}^{(n+1)}, \boldsymbol{f}_d^{(n+1)}, \boldsymbol{\alpha}^{(n+1)}) \\ = J_0(\boldsymbol{\alpha}^{(n+1)}) + \lambda \|\mathbf{y} - \boldsymbol{\alpha}^{(n+1)}\mathbf{P}(\boldsymbol{\theta}^{(n+1)}, \boldsymbol{f}_d^{(n+1)})\|_2^2 \\ \leq S_0(\boldsymbol{\alpha}^{(n)}|\boldsymbol{\alpha}^{(n)}) - S_0(\boldsymbol{\alpha}^{(n)}|\boldsymbol{\alpha}^{(n)}) + J_0(\boldsymbol{\alpha}^{(n)}) + \\ \lambda \|\mathbf{y} - \boldsymbol{\alpha}^{(n)}\mathbf{P}(\boldsymbol{\theta}^{(n)}, \boldsymbol{f}_d^{(n)})\|_2^2 \\ = J_\lambda(\boldsymbol{\theta}^{(n)}, \boldsymbol{f}_d^{(n)}, \boldsymbol{\alpha}^{(n)}). \end{aligned} \quad (31)$$

Equ. (31) means that decreasing the surrogate function  $S_\lambda(\boldsymbol{\theta}, \boldsymbol{f}_d, \boldsymbol{\alpha}|\boldsymbol{\alpha}^{(n)})$  indeed decreases  $J_\lambda(\boldsymbol{\theta}, \boldsymbol{f}_d, \boldsymbol{\alpha})$ , which guarantees the effectiveness of optimizing (29). Therefore, we only need to minimize the surrogate function  $S_\lambda(\boldsymbol{\theta}, \boldsymbol{f}_d, \boldsymbol{\alpha}|\boldsymbol{\alpha}^{(n)})$ . Then, for the given  $\boldsymbol{\theta}$  and  $\boldsymbol{f}_d$ , the optimal value of  $\boldsymbol{\alpha}$  can be immediately derived as

$$\boldsymbol{\alpha}^*(\boldsymbol{\theta}, \boldsymbol{f}_d) = \left( \mathbf{P}^H(\boldsymbol{\theta}, \boldsymbol{f}_d) \mathbf{P}(\boldsymbol{\theta}, \boldsymbol{f}_d) + \lambda^{(-1)} \mathbf{D}^{(n)} \right)^{-1} \mathbf{P}^H(\boldsymbol{\theta}, \boldsymbol{f}_d) \mathbf{y}. \quad (32)$$

When we substitute  $\boldsymbol{\alpha}^*(\boldsymbol{\theta}, \boldsymbol{f}_d)$  into (29), the optimization are converted into

$$\begin{aligned} \min_{\boldsymbol{\theta}, \boldsymbol{f}_d} S_1(\boldsymbol{\theta}, \boldsymbol{f}_d) = C(\boldsymbol{\alpha}^{(n)}) - \mathbf{y}^H \mathbf{P}(\boldsymbol{\theta}, \boldsymbol{f}_d) \\ \left( \mathbf{P}^H(\boldsymbol{\theta}, \boldsymbol{f}_d) \mathbf{P}(\boldsymbol{\theta}, \boldsymbol{f}_d) + \lambda^{(-1)} \mathbf{D}^{(n)} \right)^{-1} \mathbf{P}^H(\boldsymbol{\theta}, \boldsymbol{f}_d) \mathbf{y}. \end{aligned} \quad (33)$$

Since  $\min_{\boldsymbol{\theta}, \boldsymbol{f}_d} S_1(\boldsymbol{\theta}, \boldsymbol{f}_d)$  is differentiable with respect to  $\boldsymbol{\theta}$  and  $\boldsymbol{f}_d$ , the gradient descent can be exploited in each iteration to derive  $\boldsymbol{\theta}$  and  $\boldsymbol{f}_d$ .

Define

$$\mathbf{Z} = \mathbf{P}(\boldsymbol{\theta}, \boldsymbol{f}_d) \mathbf{R} \mathbf{P}^H(\boldsymbol{\theta}, \boldsymbol{f}_d) \mathbf{y}, \quad (34)$$

$$\mathbf{R} = \left( \mathbf{P}^H(\boldsymbol{\theta}, \boldsymbol{f}_d) \mathbf{P}(\boldsymbol{\theta}, \boldsymbol{f}_d) + \lambda^{(-1)} \mathbf{D}^{(n)} \right)^{-1}. \quad (35)$$

Then, it can be readily derived as (36), which is shown on the top of the next page.

since it holds that

$$\frac{\partial S_1(\boldsymbol{\theta}, \boldsymbol{f}_d)}{\partial \mathbf{Z}} = \frac{\partial}{\partial \mathbf{Z}} \text{tr} \{ -\mathbf{y} \mathbf{y}^H \mathbf{Z} \} = -(\mathbf{y} \mathbf{y}^H)^T \quad (37)$$

$$\frac{\partial S_1(\boldsymbol{\theta}, \boldsymbol{f}_d)}{\partial \mathbf{Z}^*} = \frac{\partial}{\partial \mathbf{Z}^*} \text{tr} \{ -\mathbf{y} \mathbf{y}^H \mathbf{Z} \} = \mathbf{0}, \quad (38)$$

the gradient of  $S_1(\boldsymbol{\theta}, \boldsymbol{f}_d)$  corresponding to  $\theta_k$  can be derived as

$$\frac{\partial S_1(\boldsymbol{\theta}, \boldsymbol{f}_d)}{\partial \theta_k} = \text{tr} \left\{ -\mathbf{y} \mathbf{y}^H \frac{\partial \mathbf{Z}}{\partial \theta_k} \right\}, \quad (39)$$

where  $\frac{\partial \mathbf{Z}}{\partial \theta_k}$  is given by

$$\begin{aligned} \frac{\partial \mathbf{Z}}{\partial \theta_k} = \frac{\partial \mathbf{P}(\boldsymbol{\theta}, \boldsymbol{f}_d)}{\partial \theta_k} \mathbf{R} \mathbf{P}^H(\boldsymbol{\theta}, \boldsymbol{f}_d) + \mathbf{P}(\boldsymbol{\theta}, \boldsymbol{f}_d) \mathbf{R} \frac{\partial \mathbf{P}^H(\boldsymbol{\theta}, \boldsymbol{f}_d)}{\partial \theta_k} - \\ \mathbf{P}(\boldsymbol{\theta}, \boldsymbol{f}_d) \mathbf{R} \left( \frac{\partial \mathbf{P}^H(\boldsymbol{\theta}, \boldsymbol{f}_d)}{\partial \theta_k} \mathbf{P}(\boldsymbol{\theta}, \boldsymbol{f}_d) + \mathbf{P}^H(\boldsymbol{\theta}, \boldsymbol{f}_d) \frac{\partial \mathbf{P}(\boldsymbol{\theta}, \boldsymbol{f}_d)}{\partial \theta_k} \right) \\ \mathbf{R} \mathbf{P}^H(\boldsymbol{\theta}, \boldsymbol{f}_d). \end{aligned} \quad (40)$$

Moreover,  $\frac{\partial \mathbf{P}(\boldsymbol{\theta})}{\partial \theta_k}$  can be derived as

$$\frac{\partial \mathbf{P}(\boldsymbol{\theta}, \boldsymbol{f}_d)}{\partial \theta_k} = \mathbf{Q} \odot \mathbf{P}(\boldsymbol{\theta}, \boldsymbol{f}_d), \quad (41)$$

where  $\mathbf{Q} \in \mathbb{C}^{M^B PT \times K}$ , and the  $k$ -th row of  $\mathbf{Q}$  is given as (42) while the elements of other rows are all zero.

The gradient of  $S_1(\boldsymbol{\theta}, \boldsymbol{f}_d)$  corresponding to  $f_{kd}$  can be derived similarly, which is given by

$$\frac{\partial S_1(\boldsymbol{\theta}, \boldsymbol{f}_d)}{\partial f_{kd}} = \text{tr} \left\{ -\mathbf{y} \mathbf{y}^H \frac{\partial \mathbf{Z}}{\partial f_{kd}} \right\}, \quad (43)$$

where  $\frac{\partial \mathbf{Z}}{\partial f_{kd}}$  is given by

$$\begin{aligned} \frac{\partial \mathbf{Z}}{\partial f_{kd}} = \frac{\partial \mathbf{P}(\boldsymbol{\theta}, \boldsymbol{f}_d)}{\partial f_{kd}} \mathbf{R} \mathbf{P}^H(\boldsymbol{\theta}, \boldsymbol{f}_d) + \mathbf{P}(\boldsymbol{\theta}, \boldsymbol{f}_d) \mathbf{R} \frac{\partial \mathbf{P}^H(\boldsymbol{\theta}, \boldsymbol{f}_d)}{\partial f_{kd}} - \\ \mathbf{P}(\boldsymbol{\theta}, \boldsymbol{f}_d) \mathbf{R} \left( \frac{\partial \mathbf{P}^H(\boldsymbol{\theta}, \boldsymbol{f}_d)}{\partial f_{kd}} \mathbf{P}(\boldsymbol{\theta}, \boldsymbol{f}_d) + \mathbf{P}^H(\boldsymbol{\theta}, \boldsymbol{f}_d) \frac{\partial \mathbf{P}(\boldsymbol{\theta}, \boldsymbol{f}_d)}{\partial f_{kd}} \right) \\ \mathbf{R} \mathbf{P}^H(\boldsymbol{\theta}, \boldsymbol{f}_d). \end{aligned} \quad (44)$$

Moreover,  $\frac{\partial \mathbf{P}(\boldsymbol{\theta}, \boldsymbol{f}_d)}{\partial f_{kd}}$  can be derived as

$$\frac{\partial \mathbf{P}(\boldsymbol{\theta}, \boldsymbol{f}_d)}{\partial f_{kd}} = \mathbf{U} \odot \mathbf{P}(\boldsymbol{\theta}, \boldsymbol{f}_d), \quad (45)$$

$$\frac{\partial S_1(\boldsymbol{\theta}, \mathbf{f}_d)}{\partial \theta_k} = \text{tr} \left\{ \left( \frac{\partial S_1(\boldsymbol{\theta}, \mathbf{f}_d)}{\partial \mathbf{Z}} \right)^T \frac{\partial \mathbf{Z}}{\partial \theta_k} \right\} + \text{tr} \left\{ \left( \frac{\partial S_1(\boldsymbol{\theta}, \mathbf{f}_d)}{\partial \mathbf{Z}^*} \right)^T \frac{\partial \mathbf{Z}^*}{\partial \theta_k} \right\}, \quad (36)$$

$$\mathbf{q} = -j2\pi \cdot \underbrace{\left[ \text{vec} \{ [0 : M^B - 1]^T * (1 + \eta/f_c * \mathbf{0}_{L \times 1}^T) \}^T, \dots, \text{vec} \{ [0 : M^B - 1]^T * (1 + \eta/f_c * (\mathbf{P} - \mathbf{1})_{L \times 1}^T) \}^T \right]}_P \in \mathbb{C}^{M^B P L \times 1}, \quad (42)$$

---

**Algorithm 1** :Uplink channel tracking

- **Step 1:** Set  $n = 0$  and  $K = K_M$ ; initialize  $\boldsymbol{\alpha}^{(0)}$ ,  $\mathbf{f}_d$ , and  $\boldsymbol{\theta}$ ; compute  $\lambda^{(n)}$  according to (26).
  - **Step 2:** At the  $n$ -th iteration, construct the surrogate function according to (33);
  - **Step 3:** By exploiting the gradient descend, the surrogate function is optimized to find a new iterative estimate of  $\boldsymbol{\theta}$  and  $\mathbf{f}_d$ ;
  - **Step 4:** Calculate  $\boldsymbol{\alpha}^{(n)}$  according to (32), and update  $\lambda^{(n+1)}$  according to (26);
  - **Step 5:** Compute  $\gamma = \|\boldsymbol{\alpha}^{(n+1)} - \boldsymbol{\alpha}^{(n)}\|_2$ . If  $\gamma < \sqrt{\epsilon}$ , then  $\epsilon = \max \{ \frac{1}{\epsilon}, \epsilon_{\min} \}$ ;
  - **Step 6:** For  $l$  satisfying  $[\boldsymbol{\alpha}^{(n+1)}]_l < \alpha_{\min}$ , remove  $[\boldsymbol{\alpha}^{(n+1)}]_l$ ,  $[\mathbf{f}_d^{(n+1)}]_l$ , and  $[\boldsymbol{\theta}^{(n+1)}]_l$  from  $\boldsymbol{\alpha}^{(n+1)}$ ,  $\mathbf{f}_d^{(n+1)}$ , and  $\boldsymbol{\theta}^{(n+1)}$ ;
  - **Step 7:** Set  $n = n+1$ ; if  $\gamma < \gamma^S$ , and go to **Step 2**, where  $\gamma^S$  is the hard threshold as the terminating condition. Otherwise stop the iteration, and output the results.
- 

where  $\mathbf{U} \in \mathbb{C}^{MPT \times G_k}$ , and the  $k$ -th row of  $\mathbf{U}$  is given by

$$\left[ \underbrace{\mathbf{u}^T, \dots, \mathbf{u}^T}_P \right]^T, \text{ and the elements of other rows are all zero.}$$

Moreover,  $\mathbf{u}$  is given by

$$\mathbf{u} = \text{vec} \{ -1j * 2 * \pi * \mathbf{1}_{M^B \times 1} * [0 : L - 1] \} \in \mathbb{C}^{M^B L \times 1}. \quad (46)$$

The concrete steps of the proposed algorithm are displayed in Alg. 1. Since the dictionary of the GCS approach is not pre-defined, which remains unknown in the process of the parameter estimation, the proposed channel tracking method overcomes the performance degradation of the traditional on-grid CS methods due to the grid mismatch.

### B. Downlink Channel Tracking with the Angular and Doppler Shift Reciprocity

1) *Downlink Channel Representation:* According to [17], [18], the physical DOAs  $\theta_k$  are approximately identical for the uplink and downlink channel transmission, namely,

$$\theta_k^D = \theta_k, \quad (47)$$

which is called *angular reciprocity*. The angular reciprocity holds true at the case that the frequency interval between the uplink and downlink channel is within several GHz.

Meanwhile, since the relative velocity of the uplink and downlink channel are the same, the downlink Doppler shift can also be derived from the uplink one, which can be name as *Doppler shift reciprocity*. We denote the downlink channel carrier frequency and its corresponding carrier wavelength as  $f_c^D$  and  $\lambda_c^D$ . With the uplink Doppler shift  $f_{kd}$ , the downlink one can be derived as

$$f_{kd}^D = f_{kd} \frac{f_c^D}{f_c}. \quad (48)$$

Then, with both the angular and Doppler shift reciprocity, the downlink channel over all the sub-carriers can be formulated as

$$\begin{aligned} \mathbf{g}_k(f) &= \alpha_k^D \text{vec} [\mathbf{a}(\theta_k^D, f) \mathbf{b}^H(f_{kd}^D)] \\ &= \alpha_k \mathbf{p}(f_{kd}^D, \theta_k^D, f). \end{aligned} \quad (49)$$

2) *Downlink Channel Tracking:* According to (49), the only unknown parameter in the downlink channel  $\mathbf{g}_k(f)$  is the complex gain  $\alpha_k^D$ . Therefore, we only need to estimate  $\alpha_k^D$  to track the total downlink channel.

Denote the beamforming vector for user  $k$  of the  $n$ -th sub-carrier as

$$\mathbf{g}_k(n) = [\mathbf{a}^D(\theta_k^D, n)]^H, \quad (50)$$

and then overall beamforming matrix at BS can be expressed as

$$\mathbf{g}^D(n) = \sum_{k=1}^{K_i} \mathbf{g}_k(n), \quad (51)$$

where the beamforming vector  $\mathbf{g}^D(n)$  says that BS formulate beams towards DOA of the scheduled UAVs.

Denote  $s$  as the training symbol, and then we select the sub-carrier  $n$  for downlink channel tracking. The angle domain sparse channels permit UAVs with different DOAs to be trained by the same pilot sequence, and therefore the same one pilot symbol  $s$  can be simultaneous utilized to decrease the training overhead.

The received signal of the  $p$ -th UAV at the  $n$ -th sub-carrier can be expressed as

$$y_p(l, n) = \mathbf{h}_k^D(l, n)\mathbf{g}^D(n)s + \omega_k^D \\ = \mathbf{h}_k^D(l, n)\mathbf{g}_k(n)s + \sum_{k'=1, k' \neq k}^{K_i} \mathbf{h}_{k'}^D(l, n)\mathbf{g}_{k'}(n)s + \omega_k^D, \quad (52)$$

where  $\sum_{k'=1, k' \neq k}^{K_i} \mathbf{h}_{k'}^D(l, n)\mathbf{g}_{k'}(n)s$  is the interference. Nevertheless, since all the scheduled UAVs has distinct DOA, it holds that  $\sum_{k'=1, k' \neq k}^{K_i} \mathbf{h}_{k'}^D(l, n)\mathbf{g}_{k'}(n)s \approx 0$ .

Then, the  $p$ -th UAV sums the received signals from all the sub-carrier, which is given by

$$y_p(l) = \sum_{n=1}^N y_p(l, n) = N\alpha_k^D e^{-j2\pi f_{kd}^D l N_b T_s} s. \quad (53)$$

Therefore, the downlink channel complex gain can be derived as

$$\hat{\alpha}_k^D = \frac{y_p(l)}{N e^{-j2\pi f_{kd}^D l N_b T_s}}, \quad (54)$$

while the downlink channel can be reconstructed as

$$\hat{\mathbf{g}}_k(f) = \hat{\alpha}_k^D \text{vec} \left[ \mathbf{a} \left( \hat{\theta}_k^D, f \right) \mathbf{b}^H \left( \hat{f}_{kd}^D \right) \right]. \quad (55)$$

With both the angle reciprocity and Doppler shift reciprocity, the unknown estimated coefficient of each scheduled UAV at the downlink channel training period is only the complex gain, which greatly decreases the training overhead. Besides, since the beamforming is executed at BS, there is no necessity for the scheduled UAVs to know the Doppler and angle signature of themselves. In this way, the feedback cost is greatly decreased for UAV communications.

### C. Simplified DOA Tracking With Kalman Filter

Denote the inverse discrete Fourier transformation (IDFT) of the channel  $\mathbf{h}_k(l, (p+1)\eta)$  between BS and UAV  $k$  in Equ. (13) as

$$\tilde{\mathbf{h}}_k(l, (p+1)\eta) = \mathbf{F}^H \mathbf{h}_k(l, (p+1)\eta), \quad (56)$$

where  $\mathbf{F}$  is the normalized  $M^B \times M^B$  IDFT matrix with  $[\mathbf{F}]_{r,q} = e^{j\frac{2\pi}{M^B} r q} / \sqrt{M^B}$ . On the basis of (56), the  $q$ -th element of  $\tilde{\mathbf{h}}_k(l, (p+1)\eta)$  can be derived as (57), which is shown on the top of the next page.

When  $M^B$  is large, there always exists  $q$  meeting  $\frac{q}{M^B} - \frac{d \sin \theta_k}{\lambda_c} - \frac{p\eta d \sin \theta_k}{c} = 0$  for the given  $p$  and  $\theta_k$ . In this case, all the channel power is concentrated on this point  $q$ , which is given by

$$q = \frac{dM^B \sin \theta_k}{\lambda_c} + \frac{M^B p\eta d \sin \theta_k}{c}. \quad (58)$$

Equ. (58) also indicates that UAVs with different DOAs will exhibit different spatial distribution. According to (57), we can obtain

$$q_k(l) = \frac{dM}{\lambda} \sin \theta_k(l) \left( 1 + \frac{n\eta}{f_c} \right) + u_k(l), \quad (59)$$

where  $u_k(l)$  is the measurement noise with variance  $Q_{u_k}$ , and Equ. (59) can be named as the *measurement equation* for DOA tracking.

### Algorithm 2 : DOA Tracking Algorithm

- **Step 1:** Initialization: obtain the prior DOA information as  $\boldsymbol{\theta}_k(1) = [\theta_k(1), 0]$ ,  $\boldsymbol{\kappa}(1) = \mathbf{0}$ ;
- **Step 2:** Compute the Jacobi matrix for the system equation:  $\boldsymbol{\phi}_k(l-1) = \frac{\partial[\boldsymbol{\psi}\boldsymbol{\theta}_k(l-1)]}{\partial\boldsymbol{\theta}_k(l-1)} = \boldsymbol{\phi}$ .
- **Step 3:** Compute the Jacobi matrix for the measurement equation: According to (57), we can derive the elements of the Jacobi matrix corresponding to the  $p+1$ -th sub-carrier as  $\boldsymbol{\varpi}_{kp}(l-1) = \frac{dM}{\lambda} \frac{\partial[\sin \theta_k(l-1)(1+\frac{n\eta}{f_c})]}{\partial\theta_k(l-1)} = \frac{dM}{\lambda} \cos \theta_k(l-1) \left( 1 + \frac{n\eta}{f_c} \right)$ , and the Jacobi matrix can be stacked from  $\boldsymbol{\varpi}_{kp}(l-1)$  as  $\boldsymbol{\varpi}_k(l-1)$ .
- **Step 4:** Prediction of the system states:  $\boldsymbol{\theta}_k(l|l-1) = \boldsymbol{\phi}\boldsymbol{\theta}_k(l-1)$ ;
- **Step 5:** Minimize the predicted mean square error (MSE):  $\boldsymbol{\kappa}(l|l-1) = \boldsymbol{\phi}_k(l-1)\boldsymbol{\kappa}(l-1)\boldsymbol{\phi}_k(l-1)^H + \mathbf{Q}_{\omega_k}$ ;
- **Step 6:** Compute the Kalman gain matrix:  $\boldsymbol{\Upsilon}(\zeta) = \boldsymbol{\kappa}(l|l-1)\boldsymbol{\varpi}_k(l-1)^H[\boldsymbol{\varpi}_k(l-1)\boldsymbol{\kappa}(l|l-1)\boldsymbol{\varpi}_k(l-1)^H + Q_{u_k}]^{-1}$ ;
- **Step 7:** DOA tracking:  $\boldsymbol{\theta}_k(l) = \boldsymbol{\theta}_k(l|l-1) + \boldsymbol{\Upsilon}(l)[q_{c,k}(l) - \frac{dM \sin \theta_k(l|l-1)}{\lambda}]$ ;
- **Step 8:** Compute minimum mean square error (MMSE):  $\boldsymbol{\kappa}(l) = [\mathbf{I} - \boldsymbol{\Upsilon}(l)\boldsymbol{\varpi}_k(l)]\boldsymbol{\kappa}(l|l-1)$ ;
- **Step 9:** Go to next block  $l+1$ .

Denote  $\boldsymbol{\Psi}_k(l) = [\theta_k(l), \dot{\theta}_k(l)]$  as the system states of DOA Tracking, where  $\theta_k(l)$  and  $\dot{\theta}_k(l)$  represent DOA and angular rate of user  $k$  in block  $l$  respectively. Then, the kinematic model can be applied to characterize the variation of DOA as [19]

$$\boldsymbol{\Psi}_k(l) = \boldsymbol{\Phi}\boldsymbol{\Psi}_k(l-1) + \boldsymbol{\omega}_k(l) \\ = \begin{bmatrix} 1 & NT_s \\ 0 & 1 \end{bmatrix} \boldsymbol{\Psi}_k(l-1) + \boldsymbol{\omega}_k(l), \quad (60)$$

where  $\boldsymbol{\omega}_k(m)$  is the system noise that meets  $E[\boldsymbol{\omega}_k(m)\boldsymbol{\omega}_k^H(m)] = \mathbf{Q}_{\omega_k}$ , and (60) can be named as the *system equation* for DOA tracking.

According to (60) and (59), the DOA tracking procedure is a typical nonlinear system. In this case, extended Kalman filter (EKF) would serve as a common approach for DOA tracking, and the detailed steps are illustrated in Alg. 2.

According to Alg. 2, the DOA can be realtimely tracked by the Kalman filter based predicting and updating. Channel tracking is transmitted to tracking the Doppler information and complex gain information, which decreases the training overhead. The whole channel tracking procedure is concluded in Fig. 4. For clarity, we summarize channel tracking procedure:

- Uplink DOA, Doppler shift, and complex gain tracking;
- Uplink channel reconstruction;
- Downlink DOA and Doppler derivation with angle and Doppler shift reciprocity;
- Downlink complex gain tracking;
- Downlink channel reconstruction.

## IV. SIMULATIONS

In this section, various simulation results are provided to verify the effectiveness of the proposed method. The dimen-

$$\begin{aligned}
\left[ \tilde{\mathbf{h}}_k(l, (p+1)\eta) \right]_q &= \frac{1}{\sqrt{M^B}} \sum_{m=0}^{M^B-1} \alpha_k e^{-j2\pi f_{kd} l N_b T_s} e^{j2\pi m \left[ \frac{q}{M} - \frac{d \sin \theta_k}{\lambda_c} - \frac{p\eta d \sin \theta_k}{c} \right]} \\
&= \frac{1}{\sqrt{M^B}} \alpha_k e^{(-j2\pi f_{kd} l N_b T_s - j \frac{M^B-1}{2} \eta_k)} \frac{\sin \left( \frac{M^B 2\pi m \left[ \frac{q}{M^B} - \frac{d \sin \theta_k}{\lambda_c} - \frac{p\eta d \sin \theta_k}{c} \right]}{2} \right)}{\sin \left( \frac{2\pi m \left[ \frac{q}{M^B} - \frac{d \sin \theta_k}{\lambda_c} - \frac{p\eta d \sin \theta_k}{c} \right]}{2} \right)}. \tag{57}
\end{aligned}$$

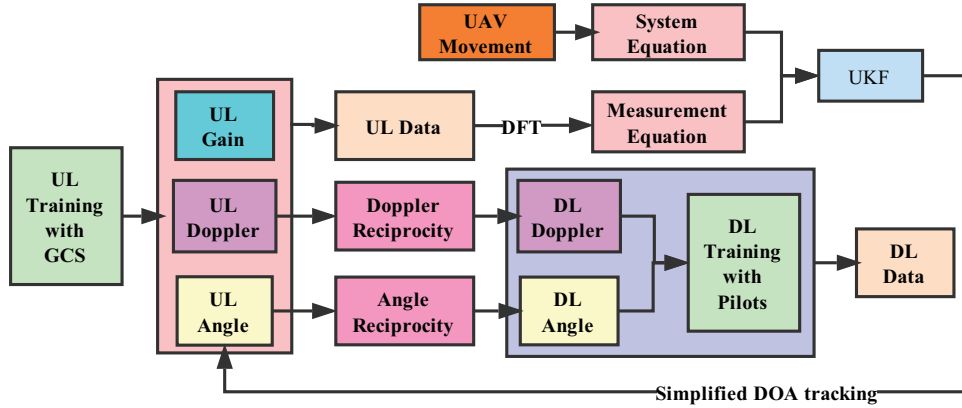


Fig. 4. Efficient channel tracking strategy for UAV communications with mmWave massive array antenna.

sion of BS antenna is  $M^B = 128$ , and the antenna spacing is set as the half of the carrier wavelength, namely,  $d = \frac{\lambda}{2}$ . The channel carrier frequency is set as  $f_c = 60$  GHz, and the bandwidth is set as  $W = 600$  MHz. There are  $K = 4$  UAVs with single antenna that are uniformly distributed in the cell. The performance criteria are set as the normalized channel gain, Doppler shift, DOA, and uplink downlink channel, which is given by

$$\text{MSE}_{\mathbf{h}_k(l)} = \frac{1}{LK} \sum_{k=1}^K \sum_{l=1}^L \frac{\|\mathbf{h}_k(l) - \hat{\mathbf{h}}_k(l)\|^2}{\|\mathbf{h}_k(l)\|^2}, \tag{61}$$

$$\text{MSE}_{\alpha_k} = \frac{1}{LK} \sum_{k=1}^K \sum_{l=1}^L \frac{\|\alpha_k - \hat{\alpha}_k\|^2}{\|\alpha_k\|^2}, \tag{62}$$

$$\text{MSE}_{f_{kd}} = \frac{1}{LK} \sum_{k=1}^K \sum_{l=1}^L \frac{\|f_{kd} - \hat{f}_{kd}\|^2}{\|f_{kd}\|^2}, \tag{63}$$

$$\text{MSE}_{\theta_k} = \frac{1}{LK} \sum_{k=1}^K \sum_{l=1}^L \frac{\|\theta_k - \hat{\theta}_k\|^2}{\|\theta_k\|^2}. \tag{64}$$

We first investigate the performance of the proposed GCS based parameter estimation method in Fig. 5. The performance metric is the normalized mean square error (MSE). It can be found that with the increase of the signal to noise ratio (SNR), MSEs of the complex gain, the Doppler shift, and DOA all decrease. Besides, we see that there are error floors of the estimated parameter due to the limited iteration step in Alg. 1.

Next, we investigate the performance of the proposed channel tracking method over SNR in Fig. 6, where the antenna number is set as  $M = 16, 32, \text{ and } 128$  respectively. It can be seen that the MSEs of the proposed GCS based channel track-

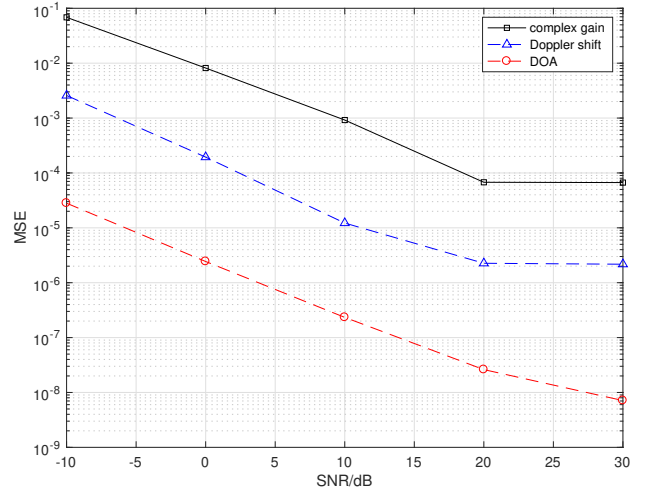


Fig. 5. The performance of parameter estimation over SNR.

ing methods decreases with the increase of SNR. Besides, with the increase of the antennas, the performance of the proposed method is enhanced, since much more antennas would bring much more spatial gain. Moreover, the conventional channel tracking method that ignores the beam squint effect would not work for UAV communications with large antenna array, which verifies the effectiveness of the proposed method.

Then, we investigate the DOA tracking performance over the time in Fig. 7, where the DFT searching method, the method in [10], and the true DOA are also displayed for comparison. It can be seen that the tendencies of all the displayed methods are consistent with the true DOA since



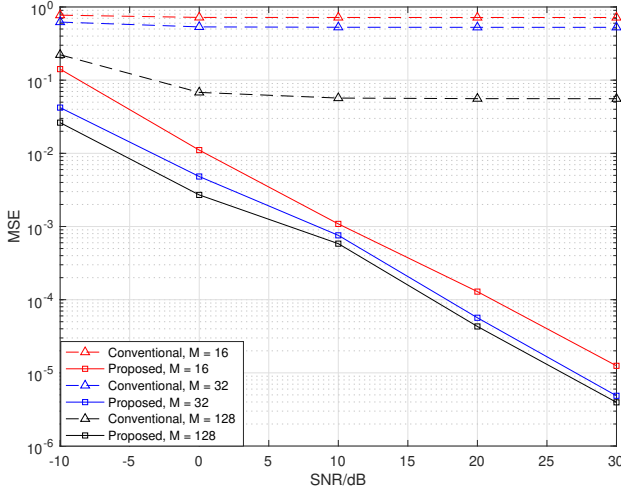


Fig. 6. The performance of the proposed channel tracking method over SNR with different number of antennas.

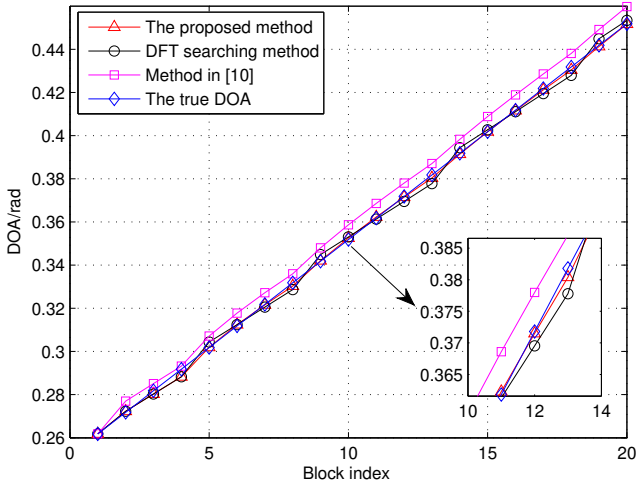


Fig. 7. The performance of the DOA tracking over SNR with different number of antennas.

the DFT of the channel could reflect the DOA distribution of the scheduled users. Besides, both the DFT searching method and the proposed method are superior to the method in [10], which neglects the beam squint effect. The performance of the proposed method is much better than the DFT searching method. The reason is that the proposed method and the DFT searching method all take the antenna selective effect into consideration, and the performance of the proposed method is further enhanced by the Kalman filter.

## V. CONCLUSIONS

In this paper, we investigated UAV communications with mmWave massive array antenna. First, we explored the UAV channel under both Doppler shift and beam squint effect. Then, we proposed an efficient channel tracking method for mmWave UAV communication systems, where the channel could be

derived by estimating DOA, Doppler shift, and complex gain information of the incident signal, respectively. The gridless compressed sensing method was exploited to track the channel parameters of UAV communications with massive antenna array. Finally, we provided various simulation results to verify the effectiveness of the proposed method over the existing ones.

## REFERENCES

- [1] Y. Zeng, R. Zhang, and T. J. Lim, "Wireless communications with unmanned aerial vehicles: opportunities and challenges," *IEEE Commun. Mag.*, vol. 54, no. 5, pp. 36–42, May 2016.
- [2] S. T. Rappaport, "Millimeter wave mobile communications for 5G cellular: it will work!" *IEEE Access*, vol. 1, no. 1, pp. 335–349, 2013.
- [3] H. Kim and Y. Kim, "Trajectory optimization for unmanned aerial vehicle formation reconfiguration," *Engineering Optimization*, vol. 41, no. 1, pp. 84–106, Jan. 2014.
- [4] D. Yang, Q. Wu, Y. Zeng, and R. Zhang, "Energy tradeoff in ground-to-UAV communication via trajectory design," *IEEE Trans. Veh. Technol.*, vol. 67, no. 7, pp. 6721–6726, July 2018.
- [5] D. Fan, F. Gao, G. Wang, Z. Zhong, and A. Nallanathan, "Angle domain signal processing aided channel estimation for indoor 60GHz TDD/FDD massive MIMO systems," *IEEE J. Select. Areas Commun.*, vol. 35, no. 9, pp. 1948–1961, Sep. 2017.
- [6] J. Ma, S. Zhang, H. Li, F. Gao, and S. Jin, "Sparse bayesian learning for the time-varying massive MIMO channels: acquisition and tracking," to be published in *IEEE Trans. Commun.*
- [7] Y. Zeng and R. Zhang, "Energy-efficient UAV communication with trajectory optimization," *IEEE Trans. Wireless Commun.*, vol. 16, no. 6, pp. 3747–3760, June 2017.
- [8] W. Mei and R. Zhang, "Uplink cooperative NOMA for cellular-connected UAV," *IEEE J. Select. Signal Process.*, vol. 13, no. 3, pp. 644–656, June 2019.
- [9] Jianpeng Ma, Shun Zhang, Hongyan Li, Nan Zhao, and Victor C.M. Leung, "Interference-alignment and soft-space-reuse based cooperative transmission for multi-cell massive mimo networks," *IEEE Trans. Wireless Commun.*, vol. 17, no. 3, pp. 1907–1922, Mar. 2018.
- [10] J. Zhao, F. Gao, W. Jia, S. Zhang, S. Jin, and H. Lin, "Angle domain hybrid precoding and channel tracking for mmWave massive MIMO systems," *IEEE Trans. Wireless Commun.*, vol. 16, no. 10, Oct. 2017, pp. 6868–6880.
- [11] B. Wang, F. Gao, S. Jin, H. Lin, and G. Ye Li "Spatial- and frequency-wideband effects in massive MIMO systems," submitted to *IEEE Trans. Signal Process.*, vol. 66, no. 13, pp. 3393–3406, May 2018.
- [12] W. Roh, J. Seol, J. Park; B. Lee, J. Lee, Y. Kim, J. Cho, K. Cheun, and F. Aryanfar, "Millimeter-Wave beamforming as an enabling technology for 5G cellular communications: theoretical feasibility and prototype results," *IEEE Commun. Mag.*, vol. 52, no. 2, Feb. 2014, pp. 106–113.
- [13] S. Rangan, T. S. Rappaport, and E. Erkip, "Millimeter-Wave cellular wireless networks: potentials and challenges," *Proc. IEEE*, vol. 102, no. 3, 2014, pp. 366–85.
- [14] Ye Li and L. J. Cimini, "Bounds on the interchannel interference of OFDM in time-varying Impairments," *IEEE Trans. Commun.*, vol. 49, no. 3, pp. 401–404, Mar. 2001.
- [15] I. R. Capoglu, Ye Li, and A. Swami, "Effect of Doppler spread in OFDM-based UWB systems," *IEEE Trans. Wireless Commun.*, vol. 4, no. 5, pp. 2559–2567, Sep. 2005.
- [16] E. J. Candes, M. B. Wakin, and S. P. Boyd, "Enhancing sparsity by reweighted l1 minimization," *J. Fourier Anal. Appl.*, vol. 14, no. 5, pp. 877–905, Dec. 2008.
- [17] Y. J. Bultitude, and T. Rautiainen, "IST-4-027756 WINNER II D1. 1.2 V1. 2 WINNER II Channel Models," 2007.
- [18] METIS, "Mobile wireless communications Enablers for the Twentytwenty Information Society," EU 7th Framework Programme project, vol. 6. ICT-317669-METIS.
- [19] Y. Zhou, P. C. Yip, and H. Leung, "Tracking the direction-of-arrival of multiple moving targets by passive arrays: algorithm," *IEEE Trans. Signal Process.*, vol. 47, no. 10, pp. 2655–2666, Oct. 1999.